Journal of Applied Electrochemistry **33**: 839–851, 2003.

Mathematical simulation of a vertically moving particle bed electrochemical cell☆

K. BOUZEK[1,*] and H. BERGMANN[2]
[1]*Department of Inorganic Technology, Institute of Chemical Technology, Technická 5, 166 28 Prague 6, Czech Republic*
[2]*Anhalt University of Applied Sciences, Bernburger Strasse 55, 06366 Köthen, Germany*
*(*author for correspondence, e-mail: bouzekk@vscht.cz)*

Received 5 November 2002; accepted in revised form 7 May 2003

Key words: cascade of reactors, electrochemical reactor, mathematical model, rotating drum, three-dimensional electrode, water treatment

Abstract

The cascade variant of the vertically moving particle bed (VMPB) cell represents a novel type of electrochemical cell for technological and wastewater treatment using a rotating three-dimensional electrode. It is characterized by a high surface area, high space–time yield and simple handling. These properties have been achieved by electrode rotation, a cascade arrangement of single rotating drums and automatic particle exchange between neighbouring rotating drums. Two types of mathematical model have been developed. They differ with regard to the degree of complexity and the numerical mathematics method used to solve the equations derived. The results obtained by the two types of model are compared. The influence of the main process parameters is studied for the model case of a single drum cell. The viability of the individual model types for evaluating the influence of the operation parameters of the cell on its performance is discussed.

List of symbols

a	specific surface area ($m^2\ m^{-3}$)
A	area (m^2)
c	concentration (mol m^{-3})
D	diffusion coefficient ($m^2\ s^{-1}$)
d	diameter (m)
E	electrode potential (V)
f	rotation frequency (Hz)
F	Faradaic constant (C mol^{-1})
i	number of increments
I	current (A)
j	current density (A m^{-2})
k	mass transfer coefficient (m s^{-1})
L	thickness (m)
M	molar mass (g mol^{-1})
Q	volumetric flow rate ($m^3\ s^{-1}$)
R	universal gas constant (J $mol^{-1}\ K^{-1}$)
Re	Reynolds number
Sc	Schmidt number
Sh	Sherwood number
T	temperature (K)
U_{cell}	cell voltage (V)
v	linear flow velocity (m s^{-1})
V	volume (m^3)
ΔV	volume of finite element (m^3)
x	coordinate (m)
Δx	finite element length (m)
z	number of electrons exchanged

Greek letters

α	charge transfer coefficient
ε	volume fraction
ζ	space–time yield (g $m^{-3}\ s^{-1}$)
η	overvoltage (V)
κ	specific conductivity (S m^{-1})
$\lambda_{1\text{-}4}$	constants, Equation 16
λ_5	constant, Equation 17
λ_6	constant, Equation 18
ν	kinematic viscosity ($m^2\ s^{-1}$)
ρ	specific resistance (Ω m)
φ	Galvani potential (V)
Φ	reaction efficiency

Subscripts

a	anodic
an	anolyte
ch	channel
bed	particle bed electrode
Cu, Cu^{2+}	copper, copper ion
c	cathodic
d	drum
e	electrode
el	electrochemical reaction

☆ This paper was originally presented at the 6th European Symposium on Electrochemical Engineering, Düsseldorf, Germany, September 2002.

g gas
H hydrogen reaction
i grid point parameter
int internal
l left-hand position
lim limiting value
Me metal
mix electrolyte between electrode particles
n number of grid points
p particle
r right-hand position
sep separator
x position on *x* coordinate
0 exchange current density

Superscripts
l left-hand position
m metallic or particle phase
r right-hand position
s solution or electrolyte phase
0 starting or inlet value

1. Introduction

During the last few decades the rapid expansion of industry has led to an increasing demand for environmentally oriented technologies. This is connected with the further development of industrial processes to meet the requirements of sustainable development [1]. Electrochemistry is capable of contributing to the broad range of technologies oriented towards environmental protection. This includes, among others, novel power sources, the selective synthesis of chemicals, the removal of impurities from process liquids and pollutants from water [2].

Electrochemical cells are well suited to meet the requirements of closed mass flow cycle technologies. In particular the elimination of the discharge of heavy metal pollutants into water has been studied intensively. This is because of their high toxicity, complications connected with their disposal in a solid form and the possibility of their remediation. A large variety of cell designs has been reported in the literature [1]. Since electrochemical processes are heterogeneous by nature, mass transfer often plays a decisive role when very dilute solutions have to be treated. From this point of view the electrochemical cells used can be divided into two main types: cells with two-dimensional (planar) and three-dimensional (3D) (sometimes called porous) electrodes. In the case of very low concentrations of contaminants in solution (usually below 1000 ppm) only 3D electrodes can provide a sufficient space-time yield defined by Equation 1,

$$\zeta = \phi_e M a_e k c^0_{Me} \quad (1)$$

where ϕ_e is the electrode reaction efficiency, M molecular weight, a_e specific electrode surface, k mass transfer coefficient and c^0_{Me} bulk concentration of metal ion.

The main advantage of the 3D electrodes is their high specific surface area. At the same time the specific hydrodynamics of the electrolyte inside the electrode provides high values of the mass transfer coefficient. On the other hand, highly non-uniform potential and current distribution inside the bed can cause efficiency losses. This problem is of particular importance for dilute solutions with low conductivity.

Numerous cell designs with fixed 3D electrodes have been reported [3–6]. The disadvantage of this experimental arrangement is that the cathode often has to be regenerated due to plugging by deposited metal. This problem was discussed extensively in our previous study [7]. A new type of cell based on a cascade of rotating drums filled with metallic particles called the vertically moving particle bed (VMPB) reactor was introduced as a possible solution [8, 9]. Two variants, a laboratory scale consisting of six drums (a) and an industrial scale consisting of seven drums (b) made of PVC and polymethylmethacrylate are shown in Figure 1. Given a suitable construction, self-classification of electrode particles according to size and automatic removal of the largest particles are possible. This allows the cell to be operated continuously. Additionally, the VMPB cell fulfils the following requirements: (i) water treatment in the pollutant concentration range 0.1–10 000 ppm, (ii) high space-time yield, (iii) minimization of the effect of the gas that has evolved, (iv) continuous transport of electrode particles and electrolyte through the cell, and (v) low cell voltage and subsequent heat evolution in the cell.

Numerous studies carried out using this type of cell have revealed its superior properties in wastewater treatment [10–12]. Current efficiency above 90% was reached for acidic solutions containing above 500 ppm Cu^{2+}. This was reduced to 30% at 100 ppm Cu^{2+}. For nickel removal from a dilute Watts-type bath a current efficiency of 40% was observed for a Ni^{2+} inlet concentration of 500 ppm. It was reduced to about 10% for 100 ppm Ni^{2+}. Correspondingly, specific energy consumption in the laboratory scale cell is around 1.5 kWh m^{-3} for reduction of the Cu^{2+} content from 500 to 150 ppm, including cell rotation and electrolyte pumping costs. Most recently, an evaluation was made of mass transfer inside the 3D cathode of this type of cell [7].

The direct transfer of laboratory results to industrial scale is only rarely possible. This is particularly true in the case of 3D electrodes, where mass-transfer and current density distribution play a decisive role. Mathematical models are necessary to test the final design of the cell before its realization. To date, mathematical models of a single rotating drum, based on equivalent schemes and accounting for various parameters, have been published [8,13]. Also an attempt to simulate a cascade of rotating drums was made [14]. Our previous work deals with the development of a macrohomogeneous model of a cascade of drums to evaluate the mass transfer coefficients inside the cell [7]. The aim

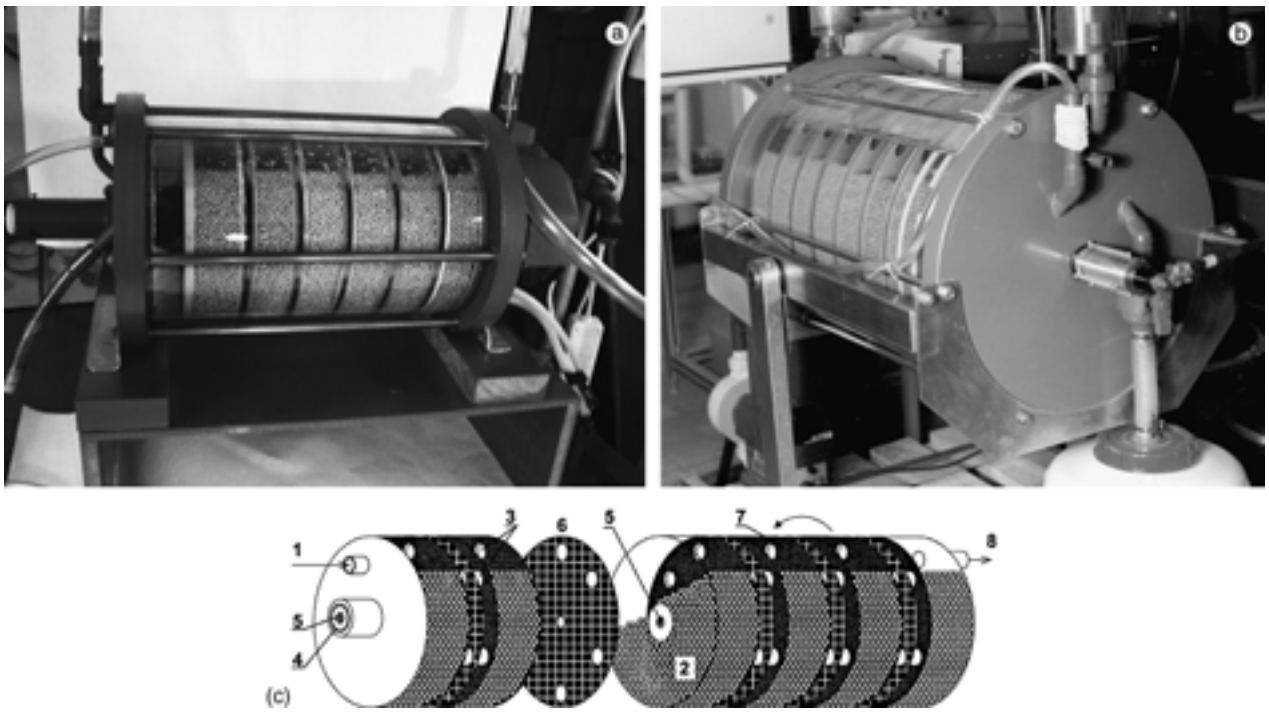

Fig. 1. (a) View of the laboratory scale cell. (External dia. 0.18 m, cell length 0.30 m, typical current load 20 A); (b) view of the industrial scale cell. (External dia. 0.60 m, typical cell length 1.10 m, typical current load 200 A); (c) schematic sketch of the arrangement of the drums, anodes, channels and separators inside the VMPB cell: 1 – electrolyte inlet, 2 – particle bed, 3 – channels between individual drums, 4 – cathode current feeder, 5 – anode current feeder, 6 – anode, 7 – separator and 8 – electrolyte outlet.

of this paper is to compare the ability of individual types of models to predict the behaviour of the VMPB cell.

2. Mathematical models

2.1. *Basic considerations*

For a better understanding of the cell function, which is necessary for the design of the model, the electrolyte and current flow patterns are schematically shown in Figure 2(a) and (b), respectively, for a hypothetical cell consisting of only four drums. The simplified electrical circuit of the cell considered in the present work is shown in Figure 2(c). A cell consisting of only three drums is shown for the sake of simplicity. The anodes are connected parallel to the current feeder. The current passes through the anolyte and the separator and enters the cathode compartment where it is consumed by the electrode reaction. In reality the electrical connections of the cathode drums are more complex. A mixture of a parallel and series arrangement is used. The current enters the cathode particles through the cathode reaction and flows further through the bodies of the individual electrodes and channels connecting the drums to the first drum where the cathode feeder is located (Figure 2(b)). If the conductivity of the cathode bed, and especially of the channels connecting the drums, is high enough (the influence of the ohmic drop between individual drums may be regarded as negligible with respect to the 3D electrode potential), the cathode drums may be considered to be electrically connected in parallel.

In the present models the current was assumed to flow to the cathode only from the anode sides directly facing it. Additionally, no electrode reaction was considered to take place inside the channels connecting the drums and no current was considered to flow through the electrolyte filling the channels. These assumptions were made because of the minor significance of the phenomena mentioned and because of their negative influence on the stability of the numerical solution of the models designed. The electric current flowing through the empty space above the particle bed was assumed to be negligible when compared with the current flowing inside the bed. On this account the influence of the radial dimension on the current distribution inside the bed can be neglected and a one-dimensional approach can be used.

In both models two parallel electrical current pathways were considered: (i) the cathode particles and (ii) the electrolyte. The potential drop in both continuums was evaluated using Equations 1 and 2, respectively.

$$\kappa^{\mathrm{m}} \frac{\mathrm{d}^2 \varphi^{\mathrm{m}}}{\mathrm{d}x^2} = -j_{\mathrm{el},x} a_{\mathrm{e}} \tag{1}$$

$$\kappa^{\mathrm{s}} \frac{\mathrm{d}^2 \varphi^{\mathrm{s}}}{\mathrm{d}x^2} = j_{\mathrm{el},x} a_{\mathrm{e}} \tag{2}$$

The value of $j_{\mathrm{el},x}$, corresponds to the current density related to the cathode reactions. The total current density is given by the sum of the partial values.

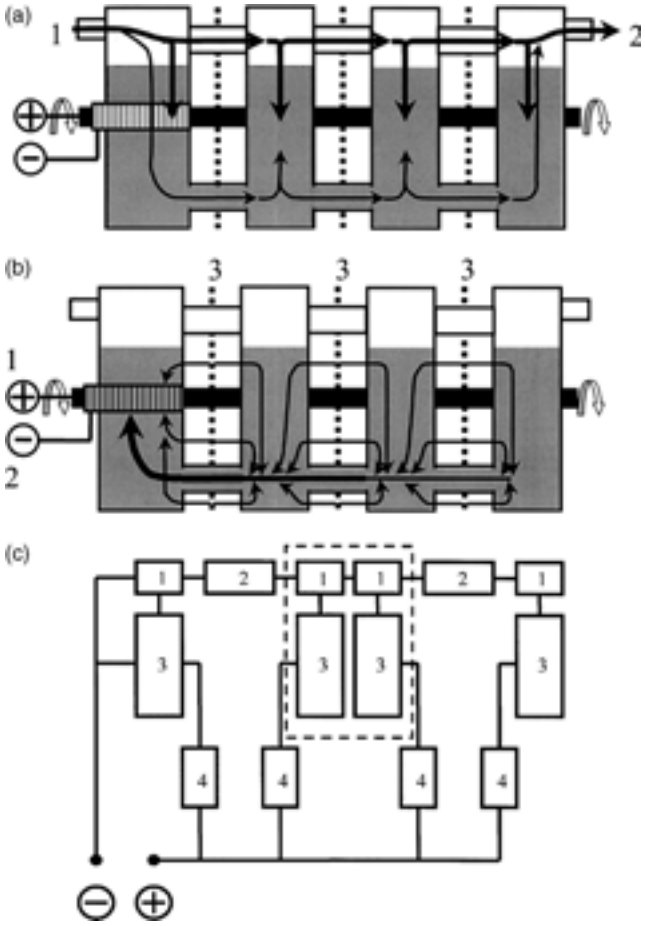

Fig. 2. (a) Simplified scheme of the hypothetical VMPB cell consisting of four rotating drums with electrolyte flow patterns: 1 – electrolyte inlet, 2 – electrolyte outlet. (b) Simplified scheme of the hypothetical VMPB cell consisting of four rotating drums with electric current flow patterns: 1 – anode current feeder, 2 – cathode current collector and 3 – anode. (c) Electric current flowchart of the three drums used in model B: 1 – electrode phase, 2 – channel between the drums, 3 – single drum, 4 – anode together with anolyte and separator.

$$j_{\mathrm{el},x} = \sum_i j_{i,x} \tag{3}$$

Copper deposition and hydrogen evolution were assumed to take place on the cathode surface. Since a diaphragm separates the anode and cathode compartments, oxygen reduction was neglected in the present case. This is a correct assumption, because oxygen present originally in the electrolyte is removed during the first pass through the cell. In the present case electrolyte is recirculated continuously. Individual current densities were evaluated by means of the following polarization curves [7].

$$j_{\mathrm{Cu},x} = \frac{-j_{0,\mathrm{Cu},x}\left[\exp\left(-\frac{\alpha_{\mathrm{Cu,c}} z_{\mathrm{Cu}} F}{RT}\eta_{\mathrm{Cu},x}\right) - \exp\left(\frac{(1-\alpha_{\mathrm{Cu,c}}) z_{\mathrm{Cu}} F}{RT}\eta_{\mathrm{Cu},x}\right)\right]}{1 - \left(\frac{j_{0,\mathrm{Cu},x}}{j_{\mathrm{lim,Cu},x}}\right) \times \exp\left(-\frac{\alpha_{\mathrm{Cu,c}} z_{\mathrm{Cu}} F}{RT}\eta_{\mathrm{Cu},x}\right)} \tag{4}$$

$$j_{\mathrm{H},x} = -j_{0,\mathrm{H}} \times \exp\left(-\frac{\alpha_{\mathrm{H,c}} z_{\mathrm{H}} F}{RT}\eta_{\mathrm{H},x}\right) \tag{5}$$

The following values of the required kinetic parameters were determined experimentally [15]: $j_{0,\mathrm{Cu}} = 1.026\ c_{\mathrm{Cu}}$, $j_{0,\mathrm{H}} = 1.26 \times 10^{-3}$ A m^{-2}, $\alpha_{\mathrm{Cu,c}} = 0.40$ and $\alpha_{\mathrm{H,c}} = 0.57$. The reversible electrode potential was evaluated using the Nernst equation. The standard redox potential of $E^{\circ}_{\mathrm{Cu^{2+}/Cu}} = 0.337$ V and $E^{\circ}_{\mathrm{H^{+}/0.5H_2}} = 0.0$ V were used [15].

The local electrode potential was evaluated on the basis of the potential difference between the solution and the electrode phase, Equation 6:

$$E = \varphi^{\mathrm{m}} - \varphi^{\mathrm{s}} \tag{6}$$

The Cu deposition limiting current density $j_{\mathrm{lim,Cu}}$ was evaluated using Equation 7:

$$j_{\mathrm{lim,Cu},x} = -kAc_{\mathrm{Cu},x} z_{\mathrm{Cu}} F \tag{7}$$

The value of mass transfer coefficient was calculated using the semi-empirical Equation 8 proposed previously [7]. That is,

$$Sh = \frac{1.09}{\varepsilon} Re_{\mathrm{p}}^{1/3} Sc^{1/3} + \frac{52.8\, Re_{\mathrm{r}}}{2498 + Re_{\mathrm{r}}} \times \{1 - \exp[-125 \times (1.04 \times 10^{-6} Re_{\mathrm{r}} + Re_{\mathrm{p}})]\} \tag{8}$$

where

$$Sh = \frac{kd_{\mathrm{p}}}{D}, \quad Re_{\mathrm{p}} = \frac{vd_{\mathrm{p}}}{v}, \quad Re_{\mathrm{r}} = \frac{fd_{\mathrm{d}}^2}{v} \tag{9}$$

Oxygen evolution was the only reaction presumed to take place on the anode surface. The Tafel equation with the following experimentally determined parameters was used to calculate the anode potential value [15].

$$E_{\mathrm{a}} = 1.41 + 0.1055 \ln j_{\mathrm{a}} \tag{10}$$

The conductivity of the electrolyte in the volume of the 3D electrode was evaluated using the Bruggemann [16] equation:

$$\rho_{\mathrm{mix}} = \rho_{\mathrm{s}}\left(1 + 1.5\frac{V_{\mathrm{m}}}{V_{\mathrm{s}}}\right) \tag{11}$$

The theory of Bockris and Kim [17] was used to estimate the conductivity of the Cu particle electrode. The conductivity of the bed was assessed to be $\kappa_{\mathrm{m}} = 4630$ to 17000 S m^{-1} for a 0.1 m high layer of Cu particles 1.0×10^{-3} to 3.5×10^{-3} m in diameter. The parameters given in [7] were used.

2.2. *Description of the models*

2.2.1. *Equivalent circuit model of one drum cell (model A)*

The approximation of the differential equations (1,2) by a network of linear elements (resistivities) is a classical

approach to the simulation of potential and current density distribution in 3D electrodes. Therefore this approach was chosen in the first instance. The structure of the equivalent circuit used to describe the problem of a single cathode drum faced by one anode is given in Figure 3.

Due to the complex nature of the electrolyte flow inside the drum, it is treated as an ideally mixed reactor. The model is based on the discretisation of the particle bed into n elements with the finite volume ΔV. Finite resistances both in the particle and the electrolyte phase can be assigned to each of these elements, as demonstrated in Figure 3. The coordinate x is set at 0 on the separator. The resulting current flowing through the individual element i may be expressed for the particle and the electrolyte phase and for the electric current flow between the phases (i.e., the electrode reaction) by Equations 12 and 13, respectively.

$$I^{m}_{i,-}\Delta x = (\varphi^{m}_{i-1} - \varphi^{m}_{i})A_c\kappa^{m} \tag{12a}$$

$$I^{m}_{i,+}\Delta x = -(\varphi^{m}_{i} - \varphi^{m}_{i+1})A_c\kappa^{m} \tag{12b}$$

$$I^{m}_{el,i} = -j_{el,i}a_e\Delta V \tag{12c}$$

$$I^{s}_{i,-}\Delta x = (\varphi^{s}_{i-1} - \varphi^{s}_{i})A_c\kappa^{s} \tag{13a}$$

$$I^{s}_{i,+}\Delta x = -(\varphi^{s}_{i} - \varphi^{s}_{i+1})A_c\kappa^{s} \tag{13b}$$

$$I^{s}_{el,i} = j_{el,i}a_e\Delta V \tag{13c}$$

$j_{el,i}$ is defined by Equation 3. A_c denotes the cross section of the particle bed and a_e indicates its specific surface. For the spherical particles it is defined by Equation 14.

$$a_e = \frac{6\varepsilon_p}{d_p} \tag{14}$$

where d_p denotes the particle diameter and ε_p particle volume fraction.

To calculate individual current values the Kirchhoff law in the form of Equation 15 was applied.

$$\sum I_i = 0 \tag{15}$$

For $x = 0$ only the current flow from the separator to the electrolyte phase and for $x = L_{bed}$ from the particle phase to the feeder are considered. The particle potential for $x = L_{bed}$ (cathode feeder) is set to 0 V.

In this type of model empirical Equation 16 was used to calculate the local value of the electrolyte conductivity. This equation was obtained by correlating experimental data for copper sulphate in sulfuric acid solution [15].

$$\kappa^{s} = \lambda_0 + \lambda_1 c_{H^+} + \lambda_2 c^2_{H^+} + \lambda_3 c_{Cu^{2+}} c_{H^+} + \lambda_4 c_{Cu^{2+}} c^2_{H^+} \tag{16}$$

Furthermore the influence of the evolving hydrogen gas on catholyte resistance was considered in order to account for the majority of factors influencing the current distribution inside the bed and to provide an accurate parametric study of a single drum cell. The value of κ^s obtained from Equation 16 was multiplied by the factor $(1 - \varepsilon_g)^{-1.5}$, where ε_g is the gas fraction inside the catholyte estimated, using Equation 17 [18]:

$$\varepsilon_g = \frac{\lambda_5 v_g^{0.5}}{(1 - \varepsilon_p)^2} \tag{17}$$

where v_g is the superficial velocity of the hydrogen gas inside the bed.

Since the electrode polarization, gas evolution intensity and subsequently the electrolyte conductivity are

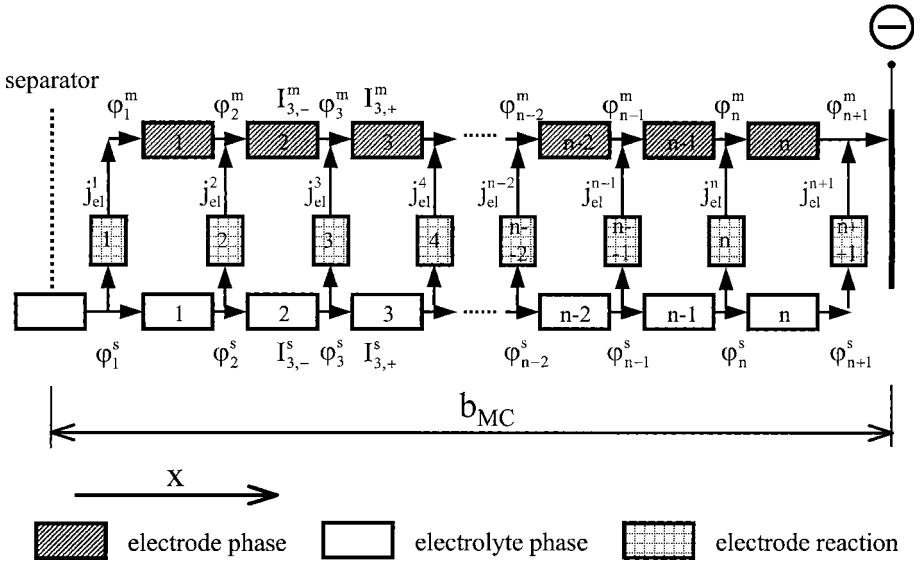

Fig. 3. Equivalent circuit for a single cell facing one anode.

interdependent, Equations 12 and 13 have to be solved iteratively until the required accuracy is reached.

A solution with inlet concentrations of $c^0_{Cu^{2+}} = 7.87$ mol m^{-3}, $c^0_{H^+} = 1000$ mol m^{-3} and electrolyte volumetric flow rate 4.5×10^{-5} m^3 s^{-1} was assumed. A particle diameter of $d_p = 2 \times 10^{-3}$ m was used, if not otherwise stated. A corresponding bed conductivity of 10^4 S m^{-1} and depth of 1.5×10^{-2} m was used. An area of 1.35×10^{-2} m^2, identical to the real laboratory scale cell, for the cross-section of the bed was assumed. A mass transfer coefficient of $k = 4.94 \times 10^{-6}$ m s^{-1} corresponded to the conditions assumed in the present calculations.

2.2.2. *Equivalent circuit model of a six-drum cascade cell (model B)*

The equivalent circuit scheme used to simulate each particulate drum was identical to the previous case, Figure 3. A model of the connection of the individual drums to form a cascade was shown in Figure 2(c).

As the particle bed conductivity is approximately three orders of magnitude higher than that of the electrolyte, the cathode drums may be considered to be connected parallel to the current feeder. This solves the problem of the cathodic current feed to the second and fifth particle bed faced by two anodes. The current enters the bed on both sides. Since a model of an ideally mixed reactor is used and parallel electrical connection is assumed, the cathode feeder may be hypothetically located in the centre of the drum. Coordinate x is set to 0 at this position. In such a case the particle bed electrode works symmetrically. The model neglects the electric current flux to the particle cathode from the side of the neighbouring anode not directly facing it. Therefore, the anodes can be hypothetically divided into two, each of which supplies current to one particle bed. The catholyte flows from drum to drum in sequence.

In this type of model the application of the electrolyte with a large excess of supporting electrolyte was assumed, that is, its conductivity was in the studied range of parameters independent of Cu^{2+} ion concentration. Since we did not deal with a system with a strong hydrogen evolution in the bed volume the influence of the gas phase on the electrolyte conductivity was neglected.

For the simulations, the geometry of the cell was identical to that used in the previous study [7]: the internal drums were 0.165 m in diameter, the rotation shaft placed in the middle of each drum 6.0×10^{-2} m in diameter. During operation of the cell, a layer of hydrogen 1.0×10^{-2} m thick formed on the top of each drum. The area of the cross section of the cathode drum filled with an electrolyte was 1.8×10^{-2} m^2, the area filled by cathode particles 1.35×10^{-2} m^2 and the total area of the channels between individual cathode drums 1.206×10^{-3} m^2. The active area of the channels filled with particles was 8.04×10^{-4} m^2, the length of each channel 1.3×10^{-2} m. A separator between the anode and cathode compartments was 8.0×10^{-4} m thick. A separator tortuosity factor of $t = 25$ was used during the simulations.

An electrolyte with the following composition was assumed: $c^0_{Cu^{2+}} = 7.87$ mol m^{-3} and $c^0_{H^+} = 100$ mol m^{-3} and $c^0_{Na_2SO_4} = 500$ mol m^{-3}. Its conductivity was 4.65 S m^{-1}. An electrolyte flow rate 7.0×10^{-5} m^3 s^{-1} and mass transfer coefficient value of $k = 3.89 \times 10^{-6}$ m s^{-1} were applied.

2.2.3. *Macrohomogeneous model (model C)*

In the case of the macrohomogeneous model differential equations (1 and 2) were integrated using the fourth order semi-implicit Runge–Kutta method. This permits a more precise study of the electrical connection of the particle cathodes to the feeder and at the same time the differential equations can be solved more accurately. In the present work a plug flow reactor model was used. The local value of the Cu^{2+} concentration was evaluated by integrating Equation 18:

$$\frac{dc_{Cu}}{dx} = \lambda_6 \times \frac{j_{Cu,x} a_c}{z_{Cu} F v} \tag{18}$$

where λ_6 is a constant. For the first drum and the right-hand region of drums 2 to 5 the value was $\lambda_6 = +1$. For the left-hand region of drums 2 to 5 and for the sixth drum it was $\lambda_6 = -1$. The current density value on the separator, necessary for evaluating the boundary conditions, was obtained by integrating the local current density values across the individual cathode beds according to Equation 19:

$$\frac{dj_{sep}}{dx} = -j_{el,x} a_c \tag{19}$$

The boundary conditions in the individual cathode drums used during simulation are discussed below.

As shown in Figure 4, the cathode current feeder passes through the whole depth of the first cathode drum. For this reason a constant potential of cathode

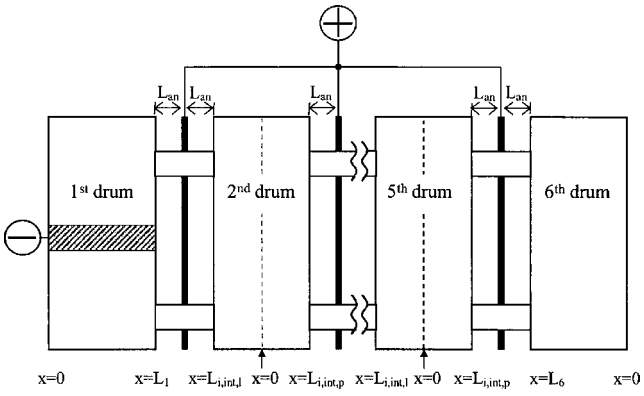

Fig. 4. Simplified scheme of the VMPB cell indicating the main dimensions used in the macrohomogeneous mathematical model – numerical integration of the differential equations.

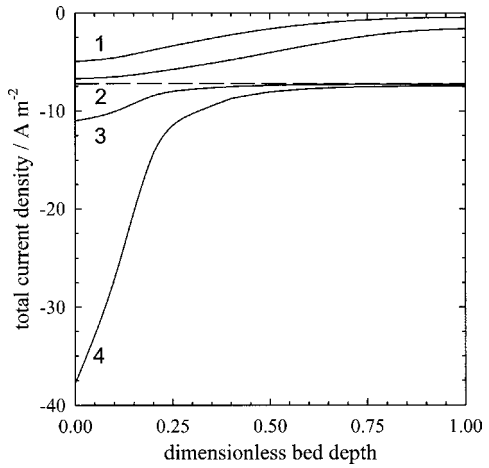

Fig. 5. Dependence of the total current distribution across the particle bed on current load. Particle bed depth 1.5×10^{-2} m; $d_p = 2 \times 10^{-3}$ m, particle bed conductivity $\kappa^m = 9800$ S m^{-1}, $c_{H_2SO_4} = 500$ mol m^{-3}, $c_{Cu^{2+}} = 7.87$ mol m^{-3}, electrolyte flow rate 4.5×10^{-5} m^3 s^{-1}, $k = 4.94 \times 10^{-6}$ m s^{-1}; current load (with respect to the separator area) (1) 50, (2) 100, (3) 200 and (4) 300 A m^{-2}. Dashed line represents the current density of mass transfer limited Cu deposition, separator is located at $x = 0$.

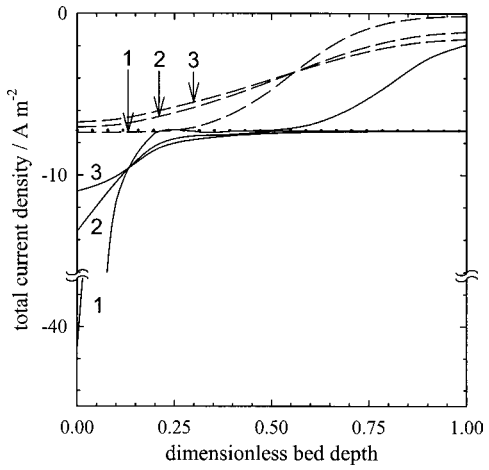

Fig. 6. Dependence of the total current distribution across the particle bed on the current load and sulphuric acid concentration. Particle bed depth 1.5×10^{-2} m; $d_p = 2 \times 10^{-3}$ m; particle bed conductivity $\kappa^m = 9800$ S m^{-1}; $c_{Cu^{2+}} = 7.87$ mol m^{-3}; electrolyte flow rate 4.5×10^{-5} m^3 s^{-1}; $k = 4.94 \times 10^{-6}$ m s^{-1}; $c_{H_2SO_4}$: (1) 50, (2) 250 and (3) 500 mol m^{-3}; current load (with respect to the separator area): dashed lines 100 A m^{-2}, full lines 200 A m^{-2}. Dotted line represents the current density of mass transfer limited Cu deposition, separator is located at $x = 0$.

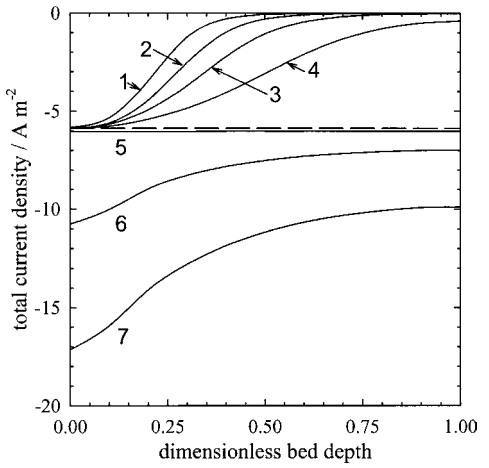

Fig. 7. Dependence of the total current distribution on the depth of the particle bed. Electrolyte flow rate 4.5×10^{-5} m^3 s^{-1}, $c_{H_2SO_4} = 500$ mol m^{-3}; $c_{Cu^{2+}} = 7.87$ mol m^{-3}; $d_p = 2 \times 10^{-3}$ m; particle bed conductivity $\kappa^m = 9800$ S m^{-1}; $k = 4.94 \times 10^{-6}$ m s^{-1}; current load (with respect to the separator area) 100 A m^{-2}; particle bed depth: (1) 5.0×10^{-2}, (2) 4.0×10^{-2}, (3) 3.0×10^{-2}, (4) 2.0×10^{-2}, (5) 1.0×10^{-2}, (6) 0.75×10^{-2} and 0.5×10^{-2} m. Dashed line represents the current density of mass transfer limited Cu deposition, separator is located at $x = 0$.

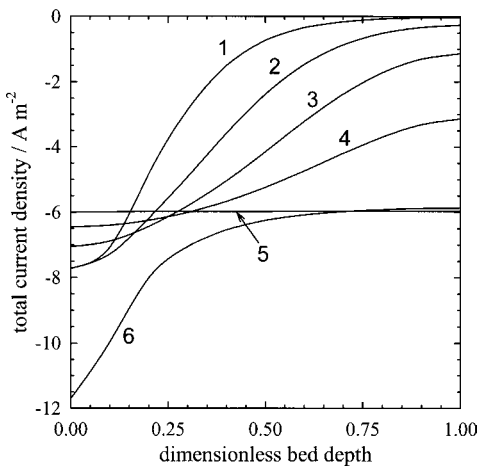

Fig. 8. Dependence of the total current distribution on the size of the particles forming the bed. Electrolyte flow rate 4.5×10^{-5} m^3 s^{-1}; $c_{H_2SO_4} = 500$ mol m^{-3}; $c_{Cu^{2+}} = 7.87$ mol m^{-3}; current load (with respect to the separator area) 100 A m^{-2}; particles diameter 1.5×10^{-2} m; d_p: (1) 1.0×10^{-3}, (2) 1.5×10^{-3}, (3) 2.0×10^{-3}, (4) 2.5×10^{-3}, (5) 3.0×10^{-3} and 3.5×10^{-3} m, separator is located at $x = 0$. Particle bed conductivities and mass transfer coefficient values used for individual particle diameters are given in Table 1.

particles φ^m was assumed here. Boundary conditions, expressed by Equations 20(a) and (b), were used to integrate Equation 2; Equation 20(c) to integrate Equation 18; and Equation 20(d) to integrate the current density on the separator, Equation 19.

$$x = 0 \quad \frac{d\varphi^s}{dx} = 0 \tag{20a}$$

$$x = L_1 \quad \varphi^s = U_{cell} - E_a - \frac{j_a}{\kappa^s} L_{an} - t\frac{j_a}{\kappa^s} L_{sep} \tag{20b}$$

$$x = 0 \qquad c_{Cu^{2+}} = c^0_{Cu^{2+}} \tag{20c}$$

$$x = 0 \quad j_a = 0 \tag{20d}$$

The positions of individual boundaries are shown in a schematic sketch of the cell in Figure 4. The third and fourth terms in Equation 20(b) correspond to the ohmic drop across the anolyte solution and the separator, respectively.

Table 1. Mass transfer coefficients and particle bed conductivity used to calculate current density distribution in dependence on particle diameter (Figures 8 and 13)

	$10^3\ d_p$/m					
	1.0	1.5	2.0	2.5	3.0	3.5
κ/S m^{-1}	4630	7200	9770	12 280	14 760	17 000
$10^6\ k$/m s^{-1}	7.76	5.89	4.95	4.39	4.01	3.74

The remaining drums are electronically contacted to the cathode current feeder only through the channels. Equation 1 has therefore to be solved as well. Anodes are located on both sides of drums 2 to 5. Therefore, the drums have to be split virtually into two regions, each collecting current from just one anode. In contrast to model B in this case these regions may not be presumed symmetrical and the position of the border ($x = 0$) has to be optimized. The following boundary conditions were applied for the left-hand regions of drums 2 to 5: for Equation 1–Equations 21(a,b), for Equation 2–Equation 21(c,d), for Equations 18 and 19–Equation 21(e,f), respectively:

$$x = L_{i,\mathrm{int,l}} \quad \varphi_i^{\mathrm{m}} = \varphi_{i-1}^{\mathrm{m}} + \Delta\varphi_{\mathrm{ch}} \tag{21a}$$

$$x = L_{i,\mathrm{int,l}} \quad \frac{\mathrm{d}\varphi_i^{\mathrm{m}}}{\mathrm{d}x} = -\frac{\mathrm{d}\varphi_{i-1}^{\mathrm{m}}}{\mathrm{d}x} \tag{21b}$$

$$x = 0 \quad \frac{\mathrm{d}\varphi^{\mathrm{s}}}{\mathrm{d}x} = 0 \tag{21c}$$

$$x = L_{i,\mathrm{int,l}} \quad \varphi^{\mathrm{s}} = U_{\mathrm{cell}} - E_{\mathrm{a}} - \frac{j_{\mathrm{a}}}{\kappa^{\mathrm{s}}} L_{\mathrm{an}} - t\frac{j_{\mathrm{a}}}{\kappa^{\mathrm{s}}} L_{\mathrm{sep}} \tag{21d}$$

$$x = L_{i,\mathrm{int},l} \quad c_{\mathrm{Cu}^{2+},i} = c_{\mathrm{Cu}^{2+},i-1} \tag{21e}$$

$$x = 0 \quad j_{\mathrm{a}} = 0 \tag{21f}$$

For the right-hand regions of these drums the following boundary conditions were used to solve differential Equations 1, 2, 18 and 19.

$$x = 0 \quad \varphi_{i,\mathrm{l}}^{\mathrm{m}} = \varphi_{i,\mathrm{r}}^{\mathrm{m}} \tag{22a}$$

$$x = 0 \quad \frac{\mathrm{d}\varphi_{i,\mathrm{l}}^{\mathrm{m}}}{\mathrm{d}x} = -\frac{\mathrm{d}\varphi_{i,\mathrm{r}}^{\mathrm{m}}}{\mathrm{d}x} \tag{22b}$$

$$x = 0 \quad \frac{\mathrm{d}\varphi^{\mathrm{s}}}{\mathrm{d}x} = 0 \tag{22c}$$

$$x = L_{i,\mathrm{int,r}} \quad \varphi^{\mathrm{s}} = U_{\mathrm{cell}} - E_{\mathrm{a}} - \frac{j_{\mathrm{a}}}{\kappa^{\mathrm{s}}} L_{\mathrm{an}} - t\frac{j_{\mathrm{a}}}{\kappa^{\mathrm{s}}} L_{\mathrm{sep}} \tag{22d}$$

$$x = 0 \quad c_{\mathrm{Cu}^{2+},i,\mathrm{l}} = c_{\mathrm{Cu}^{2+},i,\mathrm{r}} \tag{22e}$$

$$x = 0 \quad j_{\mathrm{a}} = 0 \tag{22f}$$

The position of $x = 0$ was optimized with respect to the condition given by Equation 22(d).

The sixth drum was again faced by one anode only. The following boundary conditions apply here in identical order to the previous set:

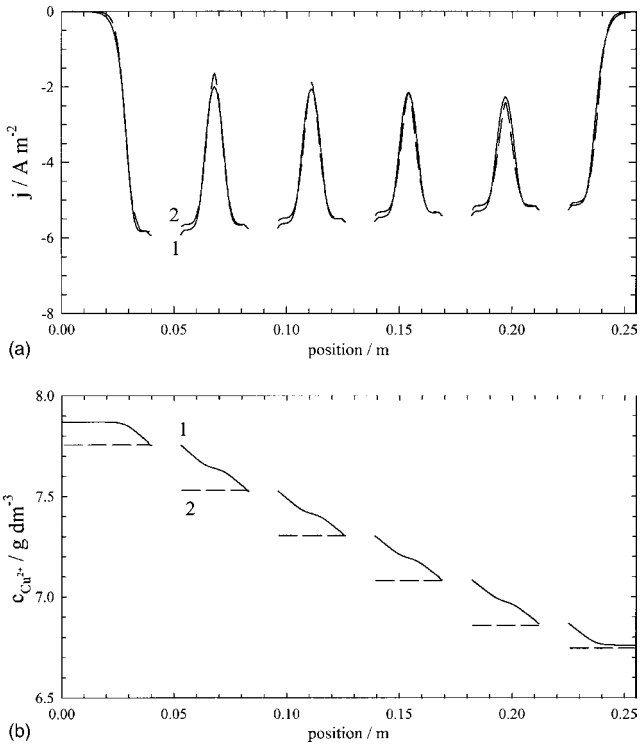

Fig. 9. Comparison of the equivalent circuit and macrohomogeneous model numerical integration of differential equations results for the cascade of rotating cathode drums. (a) Current density distribution; (b) $c_{\mathrm{Cu}^{2+}}$ distribution along the particle beds. (1) Macrohomogeneous model (C); (2) equivalent circuit model (B). Electrolyte flow rate 7.0×10^{-5} m^3 s^{-1}, $c_{\mathrm{H_2SO_4}} = 50$ mol m^{-3}; $c_{\mathrm{Cu}^{2+}} = 7.87$ mol m^{-3}; $k = 3.89 \times 10^{-6}$ m s^{-1}; current load 15 A.

$$x = L_6 \quad \varphi_6^{\mathrm{m}} = \varphi_5^{\mathrm{m}} + \Delta\varphi_{\mathrm{ch}} \tag{23a}$$

$$x = 0 \quad \frac{\mathrm{d}\varphi_6^{\mathrm{m}}}{\mathrm{d}x} = 0 \tag{23b}$$

$$x = 0 \quad \frac{\mathrm{d}\varphi^{\mathrm{s}}}{\mathrm{d}x} = 0 \tag{23c}$$

$$x = L_6 \quad \varphi^{\mathrm{s}} = U_{\mathrm{cell}} - E_{\mathrm{a}} - \frac{j_{\mathrm{a}}}{\kappa^{\mathrm{s}}} L_{\mathrm{an}} - t\frac{j_{\mathrm{a}}}{\kappa^{\mathrm{s}}} L_{\mathrm{sep}} \tag{23d}$$

$$x = L_6 \quad c_{\mathrm{Cu}^{2+},6} = c_{\mathrm{Cu}^{2+},5} \tag{23e}$$

$$x = 0 \quad j_{\mathrm{a}} = 0 \tag{23f}$$

The initial conditions were optimised using the modified Newton–Raphson method. The cell voltage corresponding to the current load was optimized to fit the experimental conditions using the DNEQNF routine with a modified Powell hybrid algorithm and a finite difference to Jacobian [19].

Cell construction and electrolyte composition and conductivity identical to that given in Section 2.2.2 were assumed. The mass transfer coefficient values were calculated using Equation 8. To obtain the mass transfer coefficient the electrolyte flow rate inside the particle bed had to be evaluated. The equations derived in [7] were used.

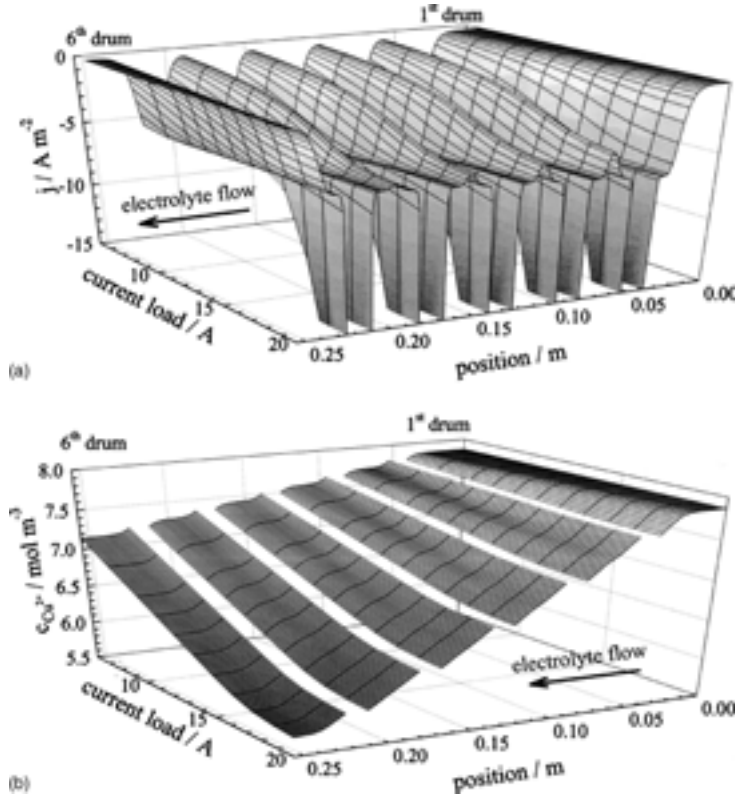

Fig. 10. Dependence of (a) total current distribution and (b) Cu^{2+} ion concentration along the cascade of electrodes on the current load. Cell parameters are given in Section 2.2.3; $c^0_{Cu^{2+}} = 7.87$ mol m^{-3}; electrolyte flow rate 4.25×10^{-5} m^3 s^{-1}; $k = 4.19 \times 10^{-6}$ m s^{-1}.

3. Results and discussion

3.1. *Single drum cell model (model A)*

During the initiation of this study model A was used in order to perform a parametric study of the single drum cell equipped with one anode only. This provides an insight into the behaviour of the particle bed and facilitates an analysis of the results obtained later on for the cell consisting of a cascade of six drums.

First, the dependence of the current density distribution across the particle bed subject to current load and electrolyte conductivity was studied. The results are shown in Figure 5. The total current density distribution manifests typical behaviour. For the lower current loads process efficiency with respect to copper deposition is high, but utilization of the bed is quite low. With increasing current loads the bed is utilized to an increasing extent. An optimal situation is reached at a current load of 200 A m^{-2}, where practically the complete bed works in the limiting current density regime of copper deposition. At the same time hydrogen evolution does not yet represent an important part of the overall current. If this level is exceeded, bed utilisation does not increase further. However, due to the commencement of intensive hydrogen evolution near the separator the efficiency of the process is substantially reduced. The irregularities in current distribution are caused by differences in the conductivities of the electrolyte and particle bed.

The influence of the sulfuric acid concentration in the electrolyte (i.e., electrolyte conductivity) for the two various current loads is depicted in Figure 6. The influence of electrolyte conductivity increases strongly with current load. As expected, reduced sulfuric concentration (and subsequently electrolyte conductivity) results in less uniform current distribution. This is more pronounced for the higher current load studied (200 A m^{-2}), where hydrogen evolution becomes important and thus allows exponential growth of current density near the separator.

Another important parameter is the thickness of the bed. If it is too thin, low conversion of the electroactive species is attained within a single pass. On the other hand, deep beds are characterised by nonuniform current distribution and low bed utilization. A comparison of the current distribution calculated for bed depths ranging from 0.5×10^{-2} to 5.0×10^{-2} m at constant current load is given in Figure 7. The Figure demonstrates that, in the range of the parameter values under study, an optimal bed depth exists providing regular utilization of the bed and high current efficiency. For the particular set of parameters used in the present case this is 1.0×10^{-2} m.

An important advantage of the VMPB reactor is the self-classification of particles according to size. With a proper configuration this results in differing particle diameters for each particular drum. The simulation performed gave the influence of particle size on current density distribution for a constant current load. The

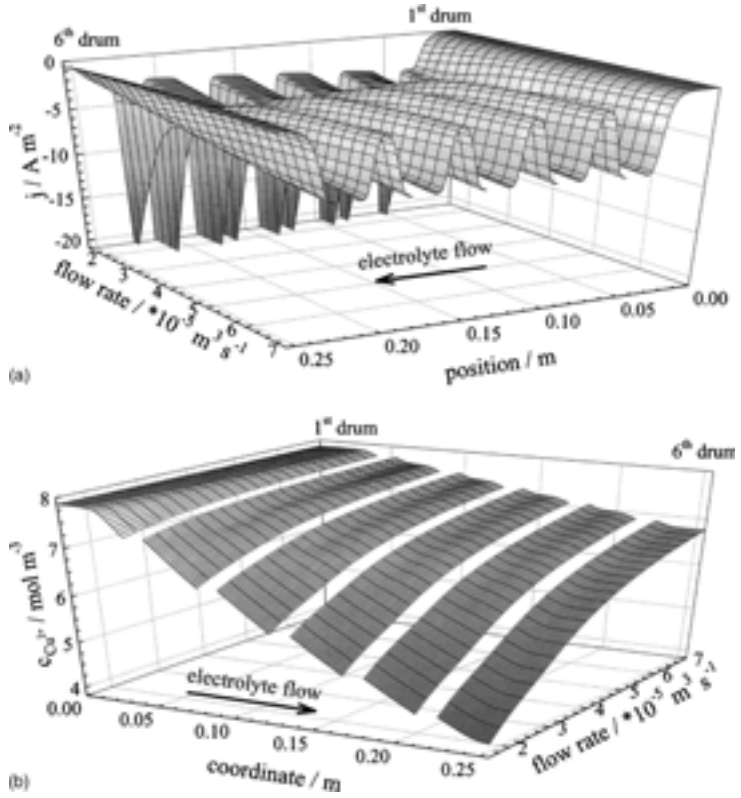

Fig. 11. Dependence of (a) total current distribution and (b) Cu^{2+} ion concentration along the cascade of electrodes on the electrolyte flow rate. Cell parameters are given in Section 2.2.3; $c^0_{Cu^{2+}} = 7.87$ mol m^{-3}; current load 15 A; mass transfer coefficient corresponding to the individual flow rates were calculated using the correlation supplied by Equation 8.

results are summarized in Figure 8. The influence of particle diameter is complex. It is directly connected not only with the specific surface of the bed, but also with the mass transfer coefficient inside the bed and with the conductivity of the bed. The values of the individual parameters used to calculate the distributions summarized in Figure 8 are given in Table 1.

It is also shown that, in the case of particle diameter, it is possible to find a diameter providing optimal utilization of the bed. For the present conditions this has a value of $d_p = 3.0 \times 10^{-3}$ m. The application of smaller particles leads to lower bed utilization. This is a consequence of the enhanced specific surface of the electrode and enhanced mass transfer coefficient. On the other hand, if the particle size is enhanced, reduced surface and mass transfer coefficients initiate intensive hydrogen evolution near the separator. This leads to lower efficiency.

It was found that the particle bed conductivity within the range used during this study (Table 1) has a negligible influence on the current distribution inside a single drum cell. For this reason it is not demonstrated here.

3.2. *Cell models with a cascade of six drums (models B and C)*

The results obtained using mathematical models B and C are compared in Figure 9. Very good agreement was obtained. The various types of model used cause a minor difference in the limiting current density on the left-hand side of the drum. Since a plug-flow model is used in the case of model C, higher concentration and subsequently higher current density at the beginning of each drum can be observed. This difference is not caused by the method used to solve Equations 1 and 2. This also provides evidence that the ohmic drop across the particle electrode is not an important factor and can be neglected in the present case. The simple type B mathematical model can be used with sufficient accuracy to describe the process of copper ion reduction inside the cascade. The effect of the ohmic drop inside the particle bed becomes apparent when intensive hydrogen evolution takes place in the cell and for beds with lower conductivity (less conductive metals, particle surface covered by an oxide film etc.).

In agreement with the single drum study, an increasing current load causes deeper penetration of the current into the particle bed. This is shown in Figure 10(a). However, after a certain limit is exceeded, a further increase in current load results in commencement of hydrogen evolution near the separators and a consequent decrease in current efficiency. This is clearly evident in Figure 10(b) which shows the dependence of the copper concentration inside the cell on the current load. Whereas with low current loads copper concentration at the outlet of the cell decreases linearly with the current load, in the region of intensive hydrogen evolution it becomes independent of this parameter.

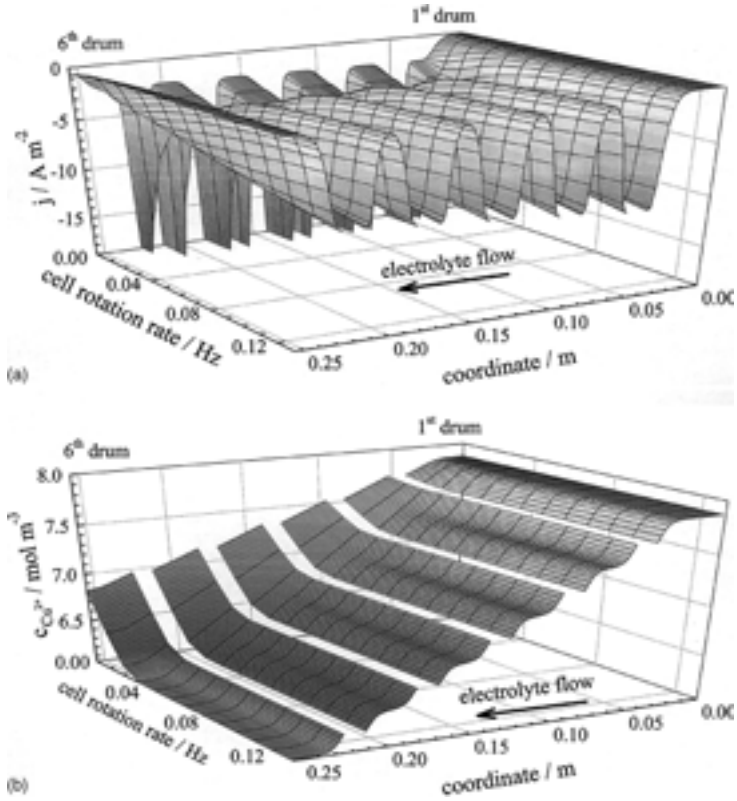

Fig. 12. Dependence of (a) total current distribution and (b) Cu^{2+} ion concentration along the cascade of the electrodes on the cell rotation rate. Cell parameters are given in Section 2.2.3; $c^0_{Cu^{2+}} = 7.87$ mol m^{-3}; current load 15 A; electrolyte flow rate 4.25×10^{-5} m^3 s^{-1}. Mass transfer coefficient corresponding to the individual rotation rates was calculated using the correlation supplied by Equation 8.

This is consistent with the fact that the cell works in a mass transfer limited regime.

Another important parameter is the electrolyte flow rate. This connects two parameters: the amount of copper ions introduced into the cell within a unit of time and the value of the mass transfer coefficient. As shown in Figure 11(a), an increase in the electrolyte flow rate results in greater non-homogeneity in the current density distribution and, at the same time, in an enhancement of the current density for copper deposition, that is, the absolute amount of copper removed from the electrolyte increases. On the other hand, Figure 11(b) clearly shows an increase in copper concentration at the outlet of the cell. The increase in mass transfer coefficient is not high enough to compensate for the increased amount of copper ions introduced into the cell. An enhanced electrolyte flow rate has a positive effect on process efficiency.

As already mentioned, an important advantage of the VMPB cell is that, in a certain range, it permits the mass transfer rate to be controlled without changing the electrolyte flow rate. This is achieved by varying the rotation rate of the drums. Figure 12(a) illustrates the influence of the rotation rate of the bed on current distribution. In this case, too, the enhanced rotation rate of the bed increases the Cu^{2+} reduction current densities inside the bed. In contrast to the previous case, however, enhanced current density simultaneously results in a decrease in copper outlet concentration, as shown in Figure 12(b). This is caused by the fact that the amount of copper introduced into the cell remains constant and does not change with the mass transfer coefficient value. This permits the effective control of copper concentration on the outlet of the cell by using appropriate electrolyte flow and cell rotation rates.

A further important advantage of the VMPB cell is the ability to self-classify particles according to size. Particle diameter does not only influence the mass transfer coefficient value, but also estimates the specific surface of the cathode. Figure 13(a) shows the current density distribution inside the VMPB cell with drums filled with particles of different diameter for two different copper inlet concentrations. Differences in the specific electrode surface between the individual drums result in different behaviour with respect to current density distribution. Whereas at an inlet concentration of 7.87 mol m^{-3} the second drum works almost completely in a mass transfer controlled regime with slight hydrogen evolution, the fifth drum works almost completely in a kinetically controlled regime. At an inlet concentration of 4.0 mol m^{-3} the drums differ mainly with regard to the extent of hydrogen evolution. The first and last drums behave differently because the anode is located on only one side of the drum. To improve an understanding of the dependence shown the integral current load of individual drums is given in Figure 13(b). A comparison of these two Figures clearly demonstrates the importance of the specific surface of the cathode. Even in the drums

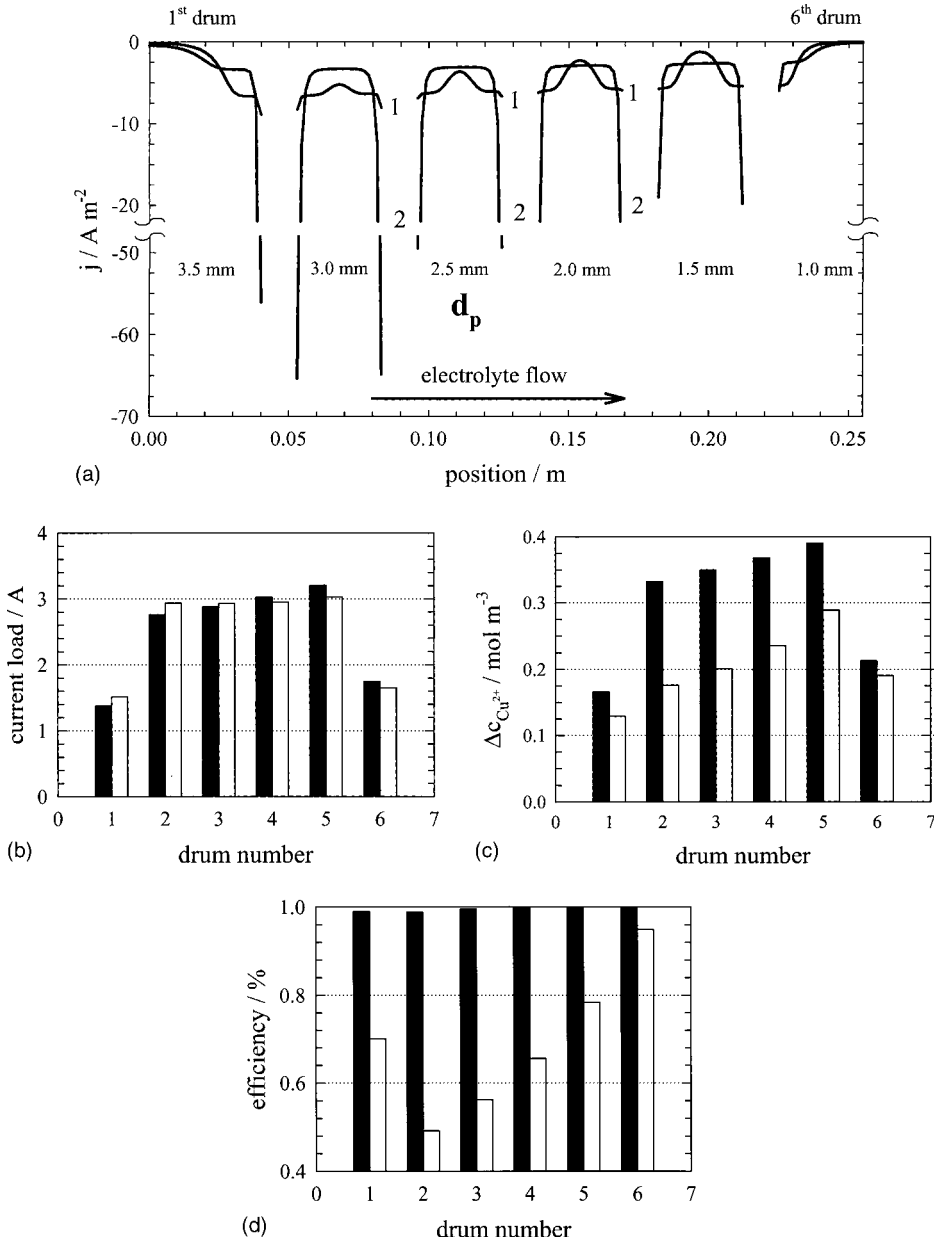

Fig. 13. (a) Total current distribution along the cascade of electrodes filled with particles of various diameter, diameter of the particles in the individual drums is shown in the Figure; $c^0_{Cu^{2+}}$: (1) 7.87 and (2) 4.00 mol m^{-3}. Current load 15 A; electrolyte flow rate 4.25×10^{-5} m^3 s^{-1}; electrode rotation rate 0.047 Hz, Mass transfer coefficient corresponding to the individual rotation rates was calculated using the correlation supplied by Equation 8 (see Table 1). (b) Distribution of the integral current load between individual drums. $c^0_{Cu^{2+}}$: (filled bars) 7.87 and (empty bars) 4.00 mol m^{-3}. (c) Decrease in Cu^{2+} ion concentration in the individual drums during the electrolyte single pass. $c^0_{Cu^{2+}}$: (filled bars) 7.87 and (empty bars) 4.00 mol m^{-3}. (d) Current efficiency of copper removal in the individual drums. $c^0_{Cu^{2+}}$: (filled bars) 7.87 and (empty bars) 4.00 mol m^{-3}.

with the largest particles the highest current density is reached, the total current load is comparable for all the drums. The total rate of copper removal is higher in the drums with smaller particles (Figure 13(c)). This difference increases with decreasing copper inlet concentration or with increasing current load. This is clearly shown by Figure 13(d), which shows the copper removal efficiency in the individual drums for two different copper inlet concentrations.

Direct comparison of model results with the experimental data is not possible, because local values of copper concentration and potential values cannot be estimated from the rotating drum interior, especially for the internal drums with the anodes on both sides. As indirect evidence a copper ion concentration decrease in the electrolyte reservoir may be used. This was provided in our previous paper for the model C [7]. Very good agreement was obtained.

4. Conclusions

Comparison of the two mathematical models has demonstrated that it is possible to neglect the influence of

ohmic potential drop across the particle electrode. This permits the use of simple model design to predict the reduction of the electroactive species on the particle cathode in the VMPB cell. In the present case the effect of the ohmic potential drop on the cathode material only influenced the hydrogen evolution current density. This effect was apparent only when the current density for copper deposition was substantially exceeded. The reason was mainly the reduced active cross section of the cell in the channels. Moreover, the particle size was found to be an important factor. The presence of the smallest particles in the last cell drum also permits more efficient treatment of more dilute solutions.

The rotation rate of the cathode drums has also been shown to be an important parameter which, to a certain extent, makes it possible to control the copper concentration in the cell outlet stream. This constitutes an important advantage of the VMPB cell compared with the classical packed bed electrode.

Acknowledgements

Financial support by the Grant Agency of the Czech Republic under project number 104/02/0664 and by the Ministry of Culture Saxony-Anhalt under project number 047A 0821 is gratefully acknowledged.

References

1. K. Jüttner, U. Galla and H. Schmieder, *Electrochim. Acta* **45** (2000) 2575.
2. L.J.J. Janssen and L. Koene, *Chem. Eng. J.* **85** (2002) 137.
3. G. Kreysa, *Chem. Ing. Tech.* **50** (1978) 332.
4. D.N. Bennion and J. Newman, *J. Appl. Electrochem.* **2** (1972) 113.
5. R.S. Wenger and D.N. Bennion, *J. Appl. Electrochem.* **6** (1976) 385.
6. J. van Zee and J. Newmann, *J. Electrochem. Soc.* **124** (1977) 706.
7. K. Bouzek, R. Chmelíková, M. Paidar and H. Bergmann, *J. Appl. Electrochem.*, 33 (2003) 205.
8. H. Bergmann, K. Hertwig and F. Nieber, *Chem. Eng. Proc.* **31** (1992) 195.
9. K. Hertwig, H. Bergmann and A. Rittel, Elektrolyseapparat mit Partikelkathoden, *DE 4210917* (28 Jan. 1993).
10. H. Bergmann, A. Rittel, *Galvanotechnik* **92** (2001) 2664.
11. H. Bergmann, A. Rittel, M. Paidar, K. Bouzek and A.S. Koparal, ISE Meeting Warsaw 2000, Abstr. no. 608.
12. A. Rittel, H. Bergmann and K. Bouzek, Galvanotechnik **92** (2002) 1747.
13. H. Bergmann, K. Hertwig and F. Nieber, 'DECHEMA-Monographien Band 125' (VCH, Weinheim, 1992).
14. H. Bergmann and K. Hertwig, *Chemische Technik* **45** (1993) 78.
15. F. Nieber, PhD. Thesis, Köthen (1992).
16. D.A.G. Bruggemann, *Ann. Phys.* **24** (1935) 636.
17. J. O'M. Bockris and J. Kim, *J. Appl. Electrochem.* **27** (1997) 890.
18. Internal report, Technische Hochschule, Köthen (1990).
19. IMSL Numerical Library (1994).